



Contents lists available at ScienceDirect

Nuclear Inst. and Methods in Physics Research, A

journal homepage: www.elsevier.com/locate/nima

eMIL: Advanced emission Mössbauer spectrometer for measurements in versatile conditions

Dmitry V. Zyabkin^{a,b,*}, Ulrich Vetter^a, Fredericus M.A. Linderhof^b, Haraldur P. Gunnlaugsson^c, Peter Schaaf^a^a Chair Materials for Electrical Engineering and Electronics, Institute of Materials Science and Engineering, Institute of Micro and Nanotechnologies MacroNano[®], TU Ilmenau, Gustav-Kirchhoff-Strasse 5, 98693 Ilmenau, Germany^b Department of Experimental Physics, Faculty of Science, Palacký University in Olomouc, 17. Listopadu 12, Olomouc, Czechia^c Science Institute, University of Iceland, Dunhaga 3, 107 Reykjavík, Iceland

ARTICLE INFO

Keywords:

Emission spectrometer
ISOLDE/CERN
Mössbauer
eMS
Implantation
Hyperfine structure

ABSTRACT

The current work presents a contemporary design of an advanced emission Mössbauer Spectrometer: eMIL equipped with a parallel-plate avalanche detector, which has been devised and built for the Mössbauer collaboration at ISOLDE/CERN. The setup is based on emission geometry, combined with on-line/off-line isotope implantation and provides numerous advantages over conversion electron, common emission (where isotope is deposited chemically on a sample) or transmission Mössbauer spectroscopy. eMIL is designed to measure hyperfine interactions in solids under various exposures. The implemented design overcomes limitations and improves performance and handling. In the current revision, the chamber is supplied with an UV extension — allowing to perform studies of photo-catalytic materials under external light exposure. A specifically designed motorized lid-samples-holder is fully automatized, and makes it possible to study up to 4 samples loaded in a magazine within a temperature range from RT up to 1100 K and to perform angular dependent measurements in high vacuum. This work additionally briefly describes data acquisition with additional electronic blocks, vacuum and data-acquisition system construction.

1. Introduction

Mössbauer spectroscopy is among the powerful methods to locally probe structural and electronic properties in condensed matter. The method allows to analyze and quantify various atomic surroundings, magnetic states, infield magnetic arrangements of magnetic moments and coordination symmetry. Moreover, the method allows us to obtain unique information, which is out of reach for other experimental techniques [1,2]. The Mössbauer effect is based on the recoilless nuclear emission and resonant absorption of γ -radiation in studied samples and is commonly applied for absorption and emission experiments. Most of the absorption experiments are done in transmission geometry. In this case, one has the detector placed behind a thin absorber (sample) and a spectrum is measured as a transmission from a Doppler shifted radioactive source. The resulting spectrum is recorded as a function of the relative source velocity. In emission experiments (emission Mössbauer spectroscopy or eMS) the radioactive parent isotope is usually introduced in the sample of interest by doping or implantation.

In the case of the on-line eMS experiments, isotopes are produced and implanted at facilities such as ISOLDE/CERN [3,4] and measurements may take place simultaneously alongside with implantation or

time delayed (implant and measure few minutes later) [5]. The main advantage of such studies is the amount of required parent isotope. For instance, with a $^{57}\text{Mn}^+$ beam flux of $2 \times 10^8/\text{s}$ one obtains peak implanted ion concentration varying from 2.5×10^{-4} at.% for the first measurement to total amount of 2×10^{-3} at.% when the final implantation of a sample is performed (6–7 measurements) [6]. The remarkably low concentrations assured single ion implantation and no overlap of implantation damage cascades. In transmission experiments, a common requirement is averaging near 0.05–0.1 at.% (for enriched ^{57}Fe) [1].

The low quantity and quick measuring time allow one to measure without the risk of precipitation, for instance isolated defects in diluted magnetic systems [7–10]. When the implantation is used to introduce the radioactive probe, the damage imparted on the host material invokes additional concern on the determination of the exact location of implanted atoms and their properties. Limit of the concentration for eMS studies is below the amorphization threshold, which is generally in the order of $10^{13} - 10^{14}$ ions/cm² depending on the material. When a sample is implanted with fluences below 10^{13} ions/cm², the implanted atoms cease to move in amorphous zones (clusters, of few nm). These

* Corresponding author at: Chair Materials for Electrical Engineering and Electronics, Institute of Materials Science and Engineering, Institute of Micro and Nanotechnologies MacroNano[®], TU Ilmenau, Gustav-Kirchhoff-Strasse 5, 98693 Ilmenau, Germany.

E-mail address: dmitry.zyabkin@tu-ilmenau.de (D.V. Zyabkin).

<https://doi.org/10.1016/j.nima.2020.163973>

Received 17 December 2019; Received in revised form 1 April 2020; Accepted 14 April 2020

Available online 18 April 2020

0168-9002/© 2020 The Authors. Published by Elsevier B.V. This is an open access article under the CC BY-NC-ND license

(<http://creativecommons.org/licenses/by-nc-nd/4.0/>).



Fig. 3. A photo of the current electronic rack. The flight case includes a NIM crate with data acquisition modules (SCA, MCA, velocity unit), computer, oscilloscope, HV unit.

plates, which generates a uniform electric field repelling conversion electrons away from the surface. These electrons ionize the gas between the plates thus causing a formation of avalanches moving towards the electrodes (Townsend discharge). Since there is broad distribution of the ionization and the avalanches growth — there is no collectable energy resolution.

2.1. Hardware

In the current work, the same PPAC detector is used [20]. It is placed relative to the incoming beam (at 90°). In order to remove the high energetic electrons emitted during the β^- decay a Beryllium window is placed on CF40 flange of the implantation chamber. This Beryllium filter effectively blocks electrons and X-rays, allowing γ -radiation to pass through with approximate transmission of 90%. The detector is mounted on a transducer with constant acceleration. It is directly connected to an Ortec 142PC pre-amplifier input. The incoming signal is being transferred to both an amplifier and an oscilloscope. The latter one is used for the adjusting of pulse height and amplitude. The signal is amplified and forwarded to the single channel analyzer (590A amplifier combined with timing single channel analyzer or SCA, Ortec). The output of the single channel analyzer is connected to a counter unit. It is of big importance to control the pulses' shape as well as the countrate. Any peculiar behavior may hint on possible vacuum leaks, sample absence etc. Furthermore, the signal from SCA is transmitted to a multichannel analyzer (MCA), which allows multichannel scaling data acquisition (MCA4, by FASTComTech). MCA additionally collects information from the transducer (the start and channel advance signals). After the evaluation process, the MCA transfers the signal to a PC. All data exchange with the PC is carried out via both RS-485 and USB connections (see Section 2.2). Currently, the PC is built on a quad-core i7 6700 3.40 Ghz CPU with 32 Gb of RAM. All modules (omitting MCA) are powered by NIM8301 by CAEN. The only exception is the pre-amplifier, which is powered by 4-channel N1471 (CAEN) power supply. The complete electronic rack is shown in Fig. 3.

The pumping unit is a separate part of eMIL. Due to safety reasons (i.e., one cannot open the target line when the pressure is insufficiently low) it has been automatized entirely. At the moment it consists of a

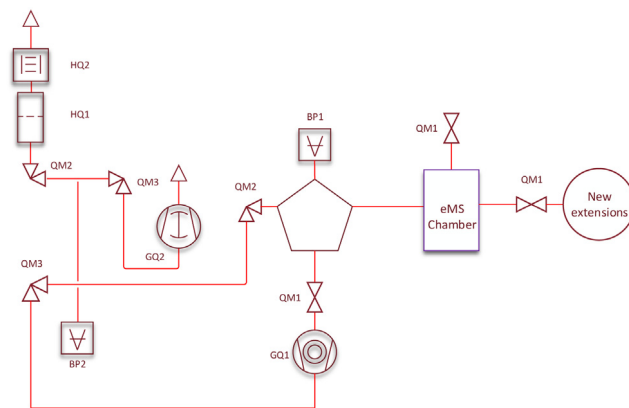


Fig. 4. Pumping unit scheme. Here QM stands for valve gates (QM1), electro-angular valves (QM2) and electro-pneumatic (QM3). GQ1 and GQ2 are turbomolecular and roots pumps, BP1 and BP2 are Pirani and Piezo gauges and HQ1-2 are particle and air filters, respectively.

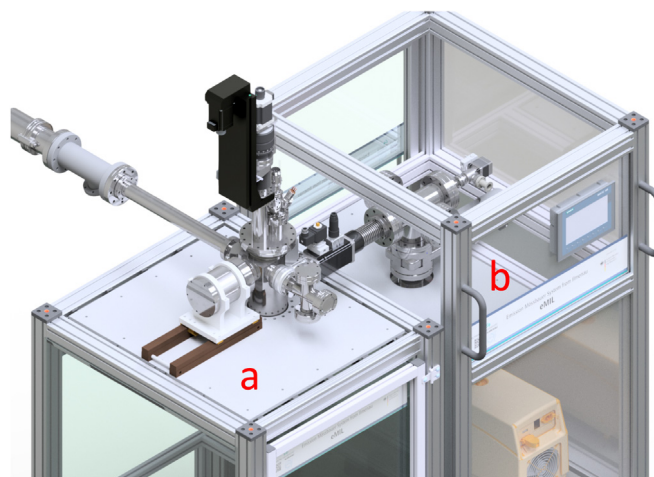


Fig. 5. The chamber unit (a), with the PPAC detector (on the rails) mounted on the transducer. The chamber itself is plugged to the pumping unit (b) via a soft bellow to minimize harmful vibrations originating from the pumps.

forepump (roots pump by Pfeiffer ACP15), turbo pump (Pfeiffer HiPace 300) and 5 valve gates and angle valves (by VAT), Pfeiffer RPT 200 and CPT 200 gauges all are controlled by RS-485 serial communication with Siemens Simatic 1212C (with SB1241RS485). Vacuum scheme is presented in Fig. 4.

This combination provides a robust base for establishing point-to-point communication via RS-485 among nodes. Besides a PC control, a human-machine-interface (Siemens Simatic KTP700) is placed on the side of the pumping unit. The units overview is shown in Fig. 5.

The remarkable flexibility of the setup is achieved by virtue of so-called lids (or sample-holders). Currently, there is solely one lid available. The lid is built on a CF100 flange with 2 CF40 ports. One CF40 flange is for the manipulation system (2 stepping motors), which allows samples to be moved along Z and Y axes (rotate and move up and down). While the second port is for the electrical feedthroughs and K-type thermocouples. The current design permits 4 samples to be measured without the need of breaking the vacuum in a temperature range from 300 to 1100 K. The temperature control is achieved with a special design and utilization of button-heaters. The heaters are made from pyrolytic boron nitride and pyrolytic graphite (by HeatWave Labs). An additional sample position is provided to a 5th sample, which can be a α -Fe foil. The optimal sample size is 1×1 cm, but additional installation of a collimator at the beam entering flange

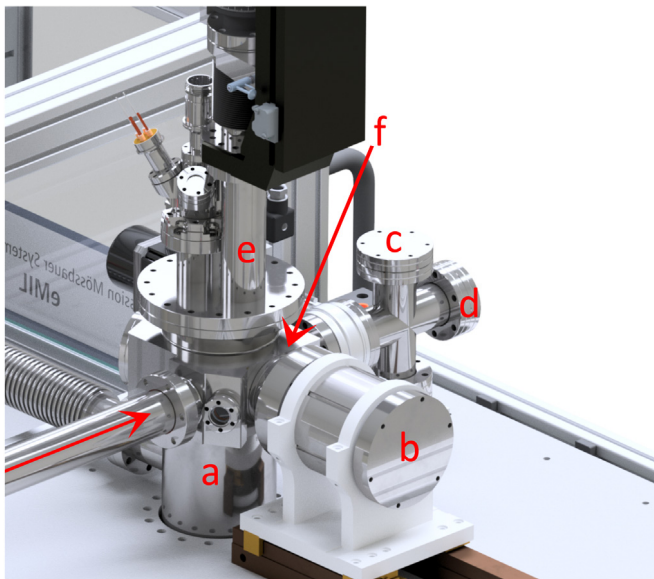


Fig. 6. The implantation chamber (a) with a hot lid mounted on top (e). On the left there is an incoming beam (marked by the arrow), next to it the quartz port, the Beryllium window (f) is placed behind the transducer (b). The transducer is equipped with a PPAC detector. On the far right is a distribution cross for chemical and magnetic extension chambers (d) and a Faraday cup mounted in a flange(c).

allows one to reduce the beam spot, and thus to implant in a small area. The rotation (Z-axis) can be employed for the determination of the angular dependence of the collected spectrum. In general, an on-line measurement (implanting and measuring) takes up to 4–5 min at $\theta_I = 30^\circ$ ($\theta_M = 60^\circ$). After this, the implantation is stopped and the sample is rotated in a way that it is placed parallel to the detector (see Fig. 6).

Last but not least, measurements as function of temperature allow the determination of the Debye–Waller factors and Debye temperatures.

At this point, the radiation during the decay is being collected for the same amount of time. Depending on the isotope the whole procedure can be repeated several times as a measure to improve the statistics. Further expansions (cryogenic, magnetic and chemical measurements) can be easily mounted on another lid, fed through the bottom flange or through the cross placed on the axis of the beam (see Figs. 2 and 5). The remote control is realized via an Arduino Uno Rev3 card, which is coupled with two of CNC single axis routers Toshiba TB6560AHQ (or 3A TB6560).

The chamber unit is based on an austenitic stainless steel (316LN ESR) tubular chamber ($\varnothing = 100$ mm). Use of this steel provides very low magnetic permeability and can withstand the harmful impact of corrosion. Everything else (CF and KF flanges, crosses) is made from 316L steel. Furthermore, when the implantation chamber was devised we had to take into account numerous factors. On the one hand, most of them were attempts to overcome the limitations one came across before, while flexibility and expanding of applications were prioritized. This resulted in a bigger chamber, with a Beryllium window which permits the usage of 2 PPAC detectors, pumping coming from the pumping station and an additional port for light experiments. The light port is inspired by the fact that one may see changes in the quadrupole splitting and isomer shift, whilst a semiconductor sample is being irradiated by a light source [22]. Additional information, including electric and vacuum schemes, drawings of the sample holder as well as a Faraday cup design, are presented in Ref. [23].

2.2. Software

In order to make the measuring experience reliable and productive two main software applications were devised and programmed. The

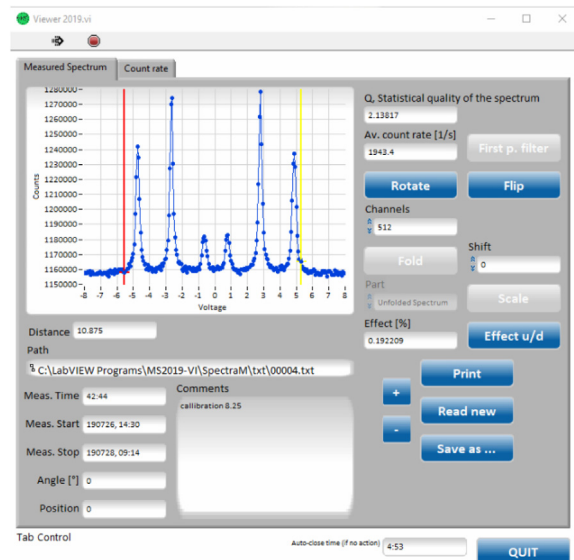


Fig. 7. eMIL's spectra viewer window, with statistical information.

first is a LabView-based data acquisition part, which is the core of eMIL and is responsible for data acquisition. In the current work we drew the main inspiration from software of a Mössbauer spectrometer built on National Instruments' solutions — Nuclear DSP System [24]. The second is a Siemens Simatic application written for a PLC-controller. Simatic can be operated remotely from a PC or directly via the human-machine-interface mounted on the pumping unit. A comprehensive description of the developed applications can be found in Ref. [23].

When a new sample is about to be measured a user can define basic parameters on the sample (velocity range, XY-relative position, temperature of the button-heaters etc.). Once acquisition has started, it can be paused and then continued later on. Additionally, software allows to directly print spectra, read previously saved measurements and convert the output data into various formats. The second tab in the Viewer Pop-Up shows a graph with the count rate over time. The preferable output format is either ASCII (.dat, txt) or binary (.ms0) which are commonly used at ISOLDE/CERN alongside with VINDA program [25] for further spectra evaluation. The viewer window is shown in Fig. 7.

A user can easily control parameters such as voltage, current and observe changes in the real time of the HV-supply and NIM crate. Several auxiliary functions were additionally implemented. With this, it becomes feasible to estimate spectral quality (Q-factor). The statistical quality of a measured Mössbauer spectrum as follows:

$$Q = \frac{\epsilon^2}{\epsilon + 2} N_\infty, \quad (1)$$

here N_∞ is the total number of the counts and ϵ stands for the resonant effect:

$$\epsilon = \frac{|N_\infty - N_0|}{N_\infty}, \quad (2)$$

where N_0 represents the number of counts at the maximum (minimum for transmission) of a resonance peak. In principle, the developed program has the flexibility to be used for Mössbauer spectroscopy in all transmission, emission or back-scattering configurations. The pumping unit is completely automatized by means of TIA Portal environment (Siemens).

3. Experimental procedure and results

In order to confirm the correct functionality in the emission geometry we have performed a couple of test measurements on both

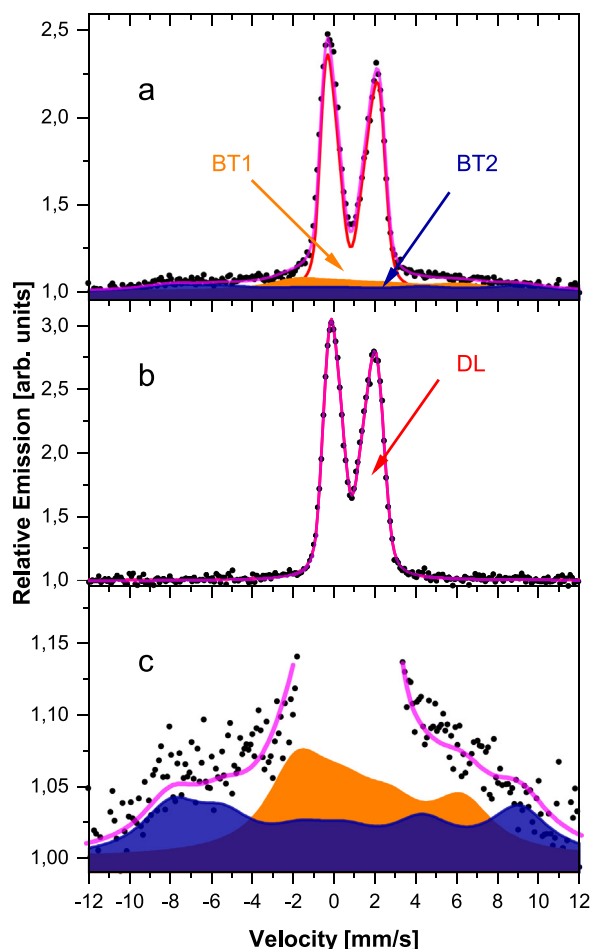


Fig. 8. ^{57}Fe emission Mössbauer spectra captured at room temperature: (a) pristine rutile; (b) rutile hydrogenated at 473 K; (c) magnified view of the pristine rutile spectrum showing the effect of the magnetic splitting.

hydrogenated and pristine TiO_2 (rutile) thin films (500 nm). The thin film were deposited onto Si substrates by radio frequency sputtering (LA 440S, VON ARDENNE), employing a TiO_2 target (99.9% FHR Anlagenbau, Germany). Prior to hydrogenation, the samples were annealed at 1173 K for 5 h to ensure their crystallization into rutile. Consequently, one sample was hydrogenated in inductively coupled hydrogen plasma (Plasma Lab 100 ICP-CVD, Oxford Instruments). The film was treated for 30 min at 2000 W at 473 K (sample temperature during the procedure).

The samples were implanted at ISOLDE/CERN after acceleration to 40 keV with ^{57}Mn ions. Emission spectrum was recorded during the implantation of a fluence 4×10^{11} ^{57}Mn ions/ cm^2 for each sample. The energy of the incoming beam results in an implantation depth up to ~ 45 nm (average 29 nm, SRIM calculations). Velocity and isomer-shift (IS) values are given relative to the center of $\alpha\text{-Fe}$ spectrum at room temperature.

Fig. 8 shows spectra of hydrogenated TiO_2 (rutile) taken at room temperature (5.7 mm/s). Pristine sample resembles results captured earlier [26], where one may notice the presence of magnetic splitting and thus were evaluated similarly. The spectrum was analyzed in terms of three components by virtue of *VINDA* program [25].

The dominating double peak (DL) in the central part was analyzed with a quadrupole split component, which was simulated as a distribution of quadrupole splittings $P(\Delta E_Q)$ [27]. A coupling between the quadrupole splitting and the isomer-shift was assumed in the evaluation of the lineshape, ($\delta = \delta_0 + \delta_1 \cdot \Delta E_Q$) where δ_1 and δ_0 were fitting variables. Here, δ_0 was used as a free parameter, δ_1 as a global parameter

(same in all spectra of the temperature series) [27]. DL was assumed to be high-spin Fe^{2+} .

Derived average isomer-shift and quadrupole splitting are $\delta_{RT} = 0.88(2)$ and $\Delta E_Q = 2.16(3)$ mm/s. The rest two components (BT1 and BT2) were analyzed with the semi-empirical Blume–Tjøn model. On the basis of current results one may assume that the behavior matches with the earlier defects annealing studies [26], where the magnetic contribution was evaluated as a paramagnetic Fe^{3+} slowly relaxing with a temperature increase.

After hydrogenation at 473 K, the spectrum changes and demonstrates no Fe^{3+} contribution. It was sufficient to employ only one Fe^{2+} component as a distribution of quadrupole splittings to reasonably fit the spectrum. Obtained isomer-shift and quadrupole splitting are $\delta_{RT} = 0.92(2)$ and $\Delta E_Q = 1.92(3)$ mm/s, respectively. The reason responsible for the absence of Fe^{3+} is likely related to a hydrogen lattice incorporation, as have been seen in the case of variously hydrogenated anatase [28]. Probably, hydrogen diffuses easily into the bulk, since the atomic probes implanted up to 45 nm are affected, thus showing no Fe^{3+} component. It is noteworthy, that annealing behavior taking place is different in anatase and rutile [23].

4. Conclusions and outlook

This paper describes the emission Mössbauer Spectrometer setup, which provides a user with great versatility and reliability. eMIL has been designed for ISOLDE/CERN and is directly connected to the GLM implantation branch. The possibility to easily perform experiments has been demonstrated. At the moment the setup supports measurements from room up to elevated (1100 K) temperatures, with the possibility to perform angular-dependent measurements and experiments under applied light irradiation. Furthermore, eMIL provides a solid ground for additional modifications. One of the ways to improve data acquisition, for instance, is the installation of the second PPAC detector. Two detectors could significantly boost the data collection time. The bottom flange can serve as the base for a DC sputtering source, if samples are going to be treated by plasma.

Declaration of competing interest

The authors declare that they have no known competing financial interests or personal relationships that could have appeared to influence the work reported in this paper.

CRediT authorship contribution statement

Dmitry V. Zybkin: Data curation, Investigation, Formal analysis, Visualization, Writing - original draft. **Ulrich Vetter:** Conceptualization, Supervision. **Fredericus M.A. Linderhof:** Software, Writing - review & editing. **Haraldur P. Gunnlaugsson:** Validation, Writing - review & editing. **Peter Schaaf:** Funding acquisition, Resources, Supervision, Writing - review & editing.

Acknowledgments

Authors are indebted to Sergii Skoblikov for his significant assistance during the spectrometer assembling. This work is supported by the German Federal Ministry of Education and Research (BMBF) projects 05K16SI1 and 05K19SI1. Fredericus M. A. Linderhof thanks the internal IGA grant of Palacký University (IGA_PrF_2020_011).

References

- [1] P. Gütlich, E. Bill, A. Trautwein, *Mössbauer Spectroscopy and Transition Metal Chemistry: Fundamentals and Applications*, Springer Berlin Heidelberg, 2010.
- [2] P. Schaaf, Mössbauer spectroscopy, in: F. Bassani, G.L. Liedl, P. Wyder (Eds.), *Encyclopedia of Condensed Matter Physics*, Elsevier, Oxford, 2005, pp. 20–31, <http://dx.doi.org/10.1016/B0-12-369401-9/01152-9>.
- [3] G. Weyer, Mössbauer Spectroscopy at ISOLDE, *Hyperfine Interact.* 129 (1) (2000) 371–390, <http://dx.doi.org/10.1023/A:1012693229011>.
- [4] K. Johnston, J. Schell, J.G. Correia, M. Deicher, H.P. Gunnlaugsson, A.S. Fenta, E. David-Bosne, A.R.G. Costa, D.C. Lupascu, The solid state physics programme at ISOLDE: recent developments and perspectives, *J. Phys. G: Nucl. Part. Phys.* 44 (10) (2017) 104001, <http://dx.doi.org/10.1088/1361-6471/aa81ac>.
- [5] H.P. Gunnlaugsson, G. Weyer, R. Mantovan, D. Naidoo, R. Sielemann, K. Bharuth-Ram, M. Fanciulli, K. Johnston, S. Ólafsson, G. Langouche, Isothermal defect annealing in semiconductors investigated by time-delayed Mössbauer spectroscopy: application to ZnO, *Hyperfine Interact.* 188 (1) (2009) 85–89, <http://dx.doi.org/10.1007/s10751-008-9893-4>.
- [6] K. Bharuth-Ram, W. Dlamini, H. Masenda, D. Naidoo, H. Gunnlaugsson, G. Weyer, R. Mantovan, T. Mølholt, R. Sielemann, S. Ólafsson, G. Langouche, K. Johnston, ^{57}Fe Mössbauer studies on $^{57}\text{Mn}^*$ implanted InP and InAs, *Nucl. Instrum. Methods Phys. Res. B* 272 (2012) 414–417, <http://dx.doi.org/10.1016/j.nimb.2011.01.112>.
- [7] H.P. Gunnlaugsson, R. Mantovan, T.E. Mølholt, D. Naidoo, K. Johnston, H. Masenda, K. Bharuth-Ram, G. Langouche, S. Ólafsson, R. Sielemann, G. Weyer, Y. Kobayashi, The ISOLDE collaboration, Mössbauer spectroscopy of ^{57}Fe in $\alpha\text{-Al}_2\text{O}_3$ following implantation of $^{57}\text{Mn}^*$, *Hyperfine Interact.* 198 (1) (2010) 5–13, <http://dx.doi.org/10.1007/s10751-010-0184-5>.
- [8] R. Mantovan, H.P. Gunnlaugsson, K. Johnston, H. Masenda, T.E. Mølholt, D. Naidoo, M. Ncube, S. Shayestehaminzadeh, K. Bharuth-Ram, M. Fanciulli, H.P. Gislason, G. Langouche, S. Ólafsson, L.M.C. Pereira, U. Wahl, P. Torelli, G. Weyer, Atomic-scale magnetic properties of truly 3d-diluted ZnO, *Adv. Electron. Mater.* 1 (1–2) (2015) 1400039, <http://dx.doi.org/10.1002/aelm.201400039>.
- [9] R. Mantovan, R. Fallica, A. Mokhles Gerami, T.E. Mølholt, C. Wiemer, M. Longo, H.P. Gunnlaugsson, K. Johnston, H. Masenda, D. Naidoo, M. Ncube, K. Bharuth-Ram, M. Fanciulli, H.P. Gislason, G. Langouche, S. Ólafsson, G. Weyer, Atomic-scale study of the amorphous-to-crystalline phase transition mechanism in GeTe thin films, *Sci. Rep.* 7 (1) (2017) 8234, <http://dx.doi.org/10.1038/s41598-017-08275-5>.
- [10] B. Qi, H. Gunnlaugsson, A.M. Gerami, H. Gislason, S. Ólafsson, F. Magnus, T. Mølholt, H. Masenda, A.T. Martín-Lueugo, A. Bonanni, P. Krastev, V. Masondo, I. Unzueta, K. Bharuth-Ram, K. Johnston, D. Naidoo, J. Schell, P. Schaaf, ^{57}Fe Mössbauer study of epitaxial TiN thin film grown on MgO(100) by magnetron sputtering, *Appl. Surf. Sci.* 464 (2019) 682–691, <http://dx.doi.org/10.1016/j.apsusc.2018.09.107>.
- [11] S. Prussin, D.I. Margolese, R.N. Tauber, Formation of amorphous layers by ion implantation, *J. Appl. Phys.* 57 (2) (1985) 180–185, <http://dx.doi.org/10.1063/1.334840>.
- [12] G. Weyer, H. Gunnlaugsson, M. Dietrich, M. Fanciulli, K. Bharuth-Ram, R. Sielemann, Creation and annealing of defect structures in silicon-based semiconductors during and after implantations at 77–500 K, *Nucl. Instrum. Methods Phys. Res. B* 206 (2003) 90–94, [http://dx.doi.org/10.1016/S0168-583X\(03\)00688-8](http://dx.doi.org/10.1016/S0168-583X(03)00688-8).
- [13] Y. Kono, C. Sanloup, *Magma Under Pressure: Advances in High-Pressure Experiments on Structure and Properties of Melts*, Elsevier Science, 2018.
- [14] M.J.G. Borge, B. Jonson, ISOLDE past, present and future, *J. Phys. G: Nucl. Part. Phys.* 44 (4) (2017) 044011, <http://dx.doi.org/10.1088/1361-6471/aa5f03>.
- [15] R. Catherall, W. Andreatza, M. Breitenfeldt, A. Dorsival, G.J. Focker, T.P. Gharsa, J. Giles T, J.-L. Grenard, F. Locci, P. Martins, S. Marzari, J. Schipper, A. Shornikov, T. Stora, The ISOLDE facility, *J. Phys. G: Nucl. Part. Phys.* 44 (9) (2017) 094002, <http://dx.doi.org/10.1088/1361-6471/aa7eba>.
- [16] M. Deicher, G. Weyer, T. Wichert, The ISOLDE Collaboration, Solid state physics at ISOLDE, *Hyperfine Interact.* 151 (1) (2003) 105–123, <http://dx.doi.org/10.1023/B:HYPE.0000020422.39876.97>.
- [17] S. Rothe, B. Marsh, C. Mattolat, V. Fedoseev, K. Wendt, A complementary laser system for ISOLDE RILIS, *J. Phys. Conf. Ser.* 312 (5) (2011) 052020, <http://dx.doi.org/10.1088/1742-6596/312/5/052020>.
- [18] V. Fedoseyev, K. Bätzner, R. Catherall, A. Evensen, D. Forkel-Wirth, O. Jonsson, E. Kugler, J. Lettry, V. Mishin, H. Ravn, G. Weyer, Chemically selective laser ion source of manganese, *Nucl. Instrum. Methods Phys. Res. B* 126 (1) (1997) 88–91, [http://dx.doi.org/10.1016/S0168-583X\(96\)01077-4](http://dx.doi.org/10.1016/S0168-583X(96)01077-4), International Conference on Electromagnetic Isotope Separators and Techniques Related to Their Applications.
- [19] V. Fedoseyev, G. Huber, U. Köster, J. Lettry, V. Mishin, H. Ravn, V. Sebastian, The ISOLDE laser ion source for exotic nuclei, *Hyperfine Interact.* 127 (1) (2000) 409–416, <http://dx.doi.org/10.1023/A:1012609515865>.
- [20] G. Weyer, Applications of parallel-plate avalanche counters in Mössbauer spectroscopy, in: *Mössbauer Effect Methodology*, vol. 10, Springer US, Boston, MA, 1976, pp. 301–319, http://dx.doi.org/10.1007/978-1-4684-8073-3_16.
- [21] R. Mantovan, M. Fanciulli, Development of a parallel-plate avalanche counter to perform conversion electron Mössbauer spectroscopy at low temperatures, *Rev. Sci. Instrum.* 78 (6) (2007) 063902, <http://dx.doi.org/10.1063/1.2745654>.
- [22] A.H. Mkrtchyan, R.P. Vardapetyan, E.M. Harutyunyan, A.V. Khachatryan, Influence of laser radiation on the Mössbauer absorption spectra of CdS (Fe^{57}) single crystal, *J. Contemp. Phys. (Armenian Academy of Sciences)* 44 (4) (2009) 191–193, <http://dx.doi.org/10.3103/S1068337209040070>.
- [23] D. Zybakin, Defect complexes interplay and its influence on the hyperfine structure of hydrogenated TiO_2 (Ph.D. thesis), TU Ilmenau, 2020.
- [24] J. Pechousek, M. Mashlan, J. Frydrych, D. Jancik, R. Prochazka, Improving detector signal processing with pulse height analysis in Mössbauer spectrometers, *Hyperfine Interact.* 175 (1) (2007) 1–8, <http://dx.doi.org/10.1007/s10751-008-9580-5>.
- [25] H.P. Gunnlaugsson, Spreadsheet based analysis of Mössbauer spectra, *Hyperfine Interact.* 237 (1) (2016) 79, <http://dx.doi.org/10.1007/s10751-016-1271-z>.
- [26] H.P. Gunnlaugsson, R. Mantovan, H. Masenda, T.E. Mølholt, K. Johnston, K. Bharuth-Ram, H. Gislason, G. Langouche, D. Naidoo, S. Ólafsson, A. Svane, G.W. and, Defect annealing in Mn/Fe-implanted TiO_2 (rutile), *J. Phys. D: Appl. Phys.* 47 (6) (2014) 065501, <http://dx.doi.org/10.1088/0022-3727/47/6/065501>.
- [27] H.P. Gunnlaugsson, A simple model to extract hyperfine interaction distributions from Mössbauer spectra, *Hyperfine Interact.* 167 (1) (2006) 851–854, <http://dx.doi.org/10.1007/s10751-006-9380-8>.
- [28] D.V. Zybakin, H.P. Gunnlaugsson, G.J. ao Nuno, K. Bharuth-Ram, B. Qi, I. Unzueta, D. Naidoo, R. Mantovan, H. Masenda, S. Ólafsson, G. Peters, J. Schell, U. Vetter, A. Dimitrova, S. Krischok, P. Schaaf, Experimental and theoretical study of electronic and hyperfine properties of hydrogenated anatase (TiO_2): defect interplay and thermal stability, *J. Phys. Chem. C* 124 (13) (2020) 7511–7522, <http://dx.doi.org/10.1021/acs.jpcc.0c00085>.